mmECG: Monitoring Human Cardiac Cycle in Driving Environments Leveraging Millimeter Wave

Xiangyu Xu* Jiadi Yu*§ Chengguang Ma† Yanzhi Ren‡ Hongbo Liu‡ Yanmin Zhu* Yi-Chao Chen* Feilong Tang*
*Department of Computer Science and Engineering, Shanghai Jiao Tong University, China
Email: {chillex, jiadiyu}@sjtu.edu.cn, {yzhu,yichao,tang-fl}@cs.sjtu.edu.cn
†Ant Financial Services Group, China
Email: chenguang.mcg@antfin.com
‡Department of Computer Science and Engineering, University of Electronic Science and Technology of China, China
Email: renyanzhi05@uestc.edu.cn, hongbo830117@gmail.com
§Corresponding Author

IEEE INFOCOM 2022 - IEEE Conference on Computer Communications | 978-1-6654-5822-1/22/$31.00 ©2022 IEEE | DOI: 10.1109/INFOCOM48880.2022.9796912

***Abstract*—The continuously increasing time spent on car trips in recent years brings growing attention to the physical and mental health of drivers on roads. As one of the key vital signs, the heartbeat is a critical indicator of drivers' health states. Most existing studies on heartbeat monitoring either require sensor attachment or could only provide sketchy heart rates. Moreover, most approaches require the subject to remain stationary or a quiet measuring environment, which is hard to apply to dynamic driving environments. In this paper, we propose a contactless cardiac cycle monitoring system, mmECG, which leverages Commercial-Off-The-Shelf mmWave radar to estimate the fine-grained heart movements of drivers in moving vehicles. By exploring the principle of mmWave signal-based sensing, we first perform studies in static environments and find the fine-grained heart movements, represented as stages of atria and ventricles in repetitive cardiac cycles, can be captured by the FMCW-based mmWave radar as phase changes in signals. Whereas in driving environments, such phase changes are caused and influenced by not only the heartbeat of drivers but also driving operations and vehicle dynamics. To further extract the minute heart movements of drivers and eliminate other influences in phase changes, we construct a movement mixture model to represent the phase changes caused by different movements, and further design a hierarchy variational mode decomposition (VMD) approach to extract and estimate the essential heart movement in mmWave signals. Finally, based on the extracted phase changes, mmECG reconstructs the cardiac cycle by estimating fine-grained movements of atria and ventricles leveraging a template-based optimization method. Experimental results involving 25 drivers in real driving scenarios demonstrate that mmECG can accurately estimate not only heart rates but also cardiac cycles of drivers in real driving environments.**

I. Introduction

Nowadays people spend more time on roads with car trips. It is reported that 87.3% of U.S. residents (ages 16 and older) spent an average of 51 minutes driving per day in 2016-2017 [1]. The considerable time on roads brings increasing attention and concern on drivers' physical and mental health, which is the cornerstone of safe traffic environments. As one of the most important vital indicators of human health, the heartbeats of human, especially the fine-grained heart movements represented as the repetitive movements of atria and ventricles in cardiac cycles, can not only reflect human body conditions such as drowsy [2], fatigue [3], but also emotional and psychological changes of human [4] [5]. Thus, monitoring the cardiac cycles of drivers in driving environments could contribute to rich categories of driving-assistance applications and healthcare services. For instance, the detection of fatigue based on cardiac cycle monitoring could raise warnings to the driver through a smartphone App, and the detection of sudden aggressive emotion from monitored heartbeat changes could help the control system of vehicles taking actions (e.g., slow down the speed) to prevent potential accidents. Therefore, it is highly desirable to provide fine-grained cardiac cycle monitoring for drivers in driving environments.

Current cardiac cycle monitoring solutions usually require daily-unavailable and intrusive infrastructures (e.g., ECG). To release the hardware requirement, recent studies employ Commercial Off-The-Shelf (COTS) devices, such as WiFi [6], RFID [7] [4], audio devices [8], etc., for low-cost and non-contact heartbeat monitoring. But due to the sensing resolution limitation, these approaches can only estimate sketchy heart rates, far from medical-level monitoring demands (i.e., cardiac cycles). Moreover, due to the lack of effective interference elimination schemes, all of these works require the target user to be relatively stationary (e.g., sitting still or sleeping) and the environment to be clean (e.g., home), neither of which can be achieved in driving environments.

To support the healthcare for driving safety, our goal is to design a non-contact and low-cost cardiac cycle monitoring system for driving environments. Among various non-contact and low-cost sensing modalities, mmWave stands out because of its fine-grained sensing capability from the short wavelength and large bandwidth. Toward this end, we aim to investigate the feasibility of leveraging mmWave signals to detect heartbeats movements for cardiac cycle monitoring in driving environments. To realize the mmWave-based cardiac cycle monitoring, we face several challenges in practice. First, the mmWave signal should be designed to be able to capture minute heart movements of human. Second, the interferences in driving environments, including driving operations and vehicle dynamics, should be eliminated from mmWave signals.

Finally, the fine-grained heart movements, i.e., stages of the atria and ventricles in each cardiac cycle, need to be reconstructed from mmWave signals.

In this paper, we first explore the principle of mmWave signal on sensing, and find that fine-grained heart movements, represented as stages of atria and ventricles, can be captured by the FMCW-based mmWave radar. Based on the observation, we propose a cardiac cycle monitoring system, *mmECG*, which leverages COTS mmWave radar to estimate fine-grained heart movements in driving environments. Specifically, we first design FMCW-based mmWave signals to reach sub-millimeter level resolution for movement detection, which could capture heart movements of drivers as phase changes in mmWave signals. With the designed mmWave signal, all movements in driving environments, including driving operations, breathing and heartbeats of drivers, dynamics of vehicles, etc., are captured as a mixed phase change in mmWave signals. Then, we propose a movement mixture model to represent the phase changes caused by all movements, and further design a hierarchy VMD approach to extract the phase change of heart movement in the mixed phase change signal mmWave signals. Finally, we propose a template-based optimization to reconstruct the cardiac cycle, i.e., fine-grained movements of atria and ventricles, based on the extracted phase changes.

We highlight our main contributions as follows:

• We design a non-contact cardiac cycle monitoring system, mmECG, which leverages COTS mmWave radars to estimate fine-grained heart movements in driving environments.

• We model diverse movements induced by heartbeats and driving environments in mmWave signals and design a hierarchy VMD to estimate the basic heart movement embedded underlying mmWave signals.

• We conduct experiments in real driving environments and the results show that mmECG achieves an average error of $0.37bpm$ for heart rate estimation, $11.2ms$ for heart rate variation estimation, and $6.8ms$ for cardiac cycle estimation.

II. Preliminary

In this section, we present the background on physiology of the human heartbeat and the principle of using mmWave signal to detect minute vibrations and movements. Then, we investigate the feasibility of capturing fine-grained heart movements with mmWave signals.

A. Background of Human Heartbeats

Human heart-beating is a physiological activity of human body, in which the heart pumps blood through the blood vessels of the circulatory system, presenting as repetitive heart movements, i.e., cardiac cycles. As illustrated in figure 1, a cardiac cycle contains 5 basic heart stages, which begins with the atria contraction, and progresses to the isovolumic contraction, ventricular ejection, isovolumic relaxation, and finally the ventricular filling [9]. Typically, the electrocardiogram (ECG) is a common approach to measure human heartbeats for diagnosing numerous cardiac abnormalities, such as cardiac

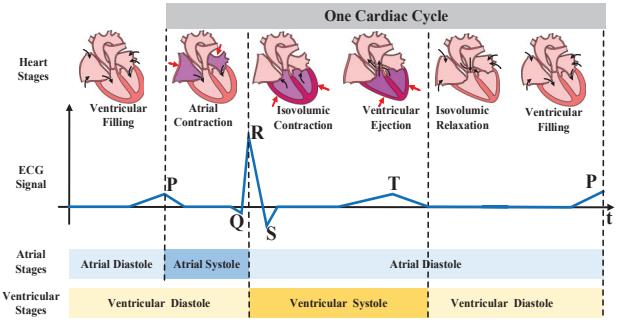

Fig. 1. Illustration of a cardiac cycle and corresponding ECG measurement.

rhythm disturbances, inadequate coronary artery blood flow, and electrolyte disturbances.

The basic principle of ECG measurement is to employ electrodes placed on the skin for detecting the electrical activity of the heart [10]. There are three key components in the ECG, i.e., P wave representing the depolarization of atria, QRS complex indicating the depolarization of ventricles, and T wave exhibiting the repolarization of ventricles [10]. And the heart stages in a cardiac cycle, divided into the stages of atria and ventricles, have a clear relationship with the three key components in the corresponding ECG measurement [11], as shown in figure 1. P wave in ECG is followed by the atrial contraction (systole), which extends until the QRS complex in ECG appears. After the QRS complex, the atria relaxes (diastole). Then, QRS complex in ECG is followed by ventricular contraction (systole), whose end is marked by the end of T wave. Also, the end of T wave indicates the beginning of ventricular relaxation (diastole).

The tight correlation between ECG and heart movements indicates that the movement of atria and ventricles, which bring chest vibrations that could be captured by mmWave, are able to provide the profound information of human heartbeats for healthcare monitoring.

B. Principle of Using mmWave to Detect Heart Activities

Millimeter wave (mmWave)-based sensing technology is developing rapidly in recent years. Because of the small wavelength, mmWave is able to sense minute movements, e.g., human heartbeat activities. Specifically, a mmWave-based FMCW radar continuously transmits chirp signals to an object, and collects the received signal. Then, the displacement Δd of the object can be calculated as $\Delta d = \frac{\lambda \Delta \phi}{4\pi}$, where λ is the wavelength associated with the average frequency of the transmitted mmWave, $\Delta\phi$ is the phase change caused by the displacement of object in the dechirped signal between the received and transmitted signals. It can be seen that a smaller wavelength (i.e., higher frequency) of the transmitted waveform leads to a better resolution for displacement detection. Thus, we leverage a $77 \sim 81GHz$ off-the-shelf mmWave radar (with one of the highest frequency range in COTS mmWave sensors) to build the system, the resolution of displacement is about $1mm$ per π phase changes in the dechirped signal, which can achieve sub-millimeter level resolution for the movement detection.

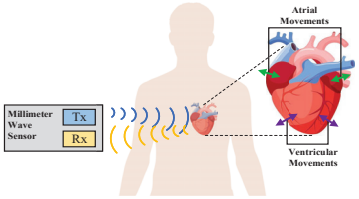

Fig. 2. Illustration of mmWave-based fine-grained heart movements detection.

Existing study [12] shows that mmWave can easily penetrate most kinds of cloth, but can hardly penetrate or be absorbed by the skin of human. So theoretically, the chest vibrations induced by heart movements, which is roughly in millimeter-level, can be captured using mmWave signal. Figure 2 illustrates the basic idea of mmWave-based fine-grained heartbeat activities detection. A mmWave radar continuously transmits FMCW signal through the transmitter end (Tx) to the region of human chest. Most of the mmWave signal is reflected by the chest, and further captured by the receiver end (Rx) of mmWave radar. During this process, the minute vibrations of chest caused by the movements of atria and ventricles are captured by the FMCW radar.

C. Feasibility of Detect Fine-grained Heart Movements

We conduct an experiment in the lab to validate the basic idea of leveraging mmWave-based FMCW radar for capturing fine-grained heart movements. In particular, we ask a volunteer to sit on a chair, with chest directly towards a mmWave radar. The distance between the radar and the volunteer is around $40cm$. Then, we generate FMCM wave whose frequency sweeps the range of $[77, 81]GHz$ to capture the heartbeat activities, during which the volunteer sits still and holds the breath to avoid the interferences of any movements other than heartbeats. Meanwhile, an ECG sensor is attached to record ECG signals as the ground truth.

Figure 3 shows the normalized phase changes of mmWave measurement and corresponding ECG measurement in $2s$, which contains three complete cardiac cycles of the volunteer. It can be seen from the figure that there are clear time relationships between mmWave and ECG measurements. Taking the second cardiac cycle as an example, there are three typical time relationships. First, the beginning time of the second increase trend in mmWave measurement, i.e., t_1, relates to the middle part of P wave in ECG, which is the beginning of atrial systole. Second, the time of the maximum value in mmWave measurement, i.e., t_2, corresponds to Q wave in ECG measurement. Since QRS complex is taken as a combination in ECG measurement and the time interval between Q wave and R wave is normally less than $0.03s$ [13], t_2 could roughly represent the end of atrial systole and the beginning of ventricular systole. Third, the time of the minimum value in mmWave measurement, i.e., t_3, corresponds to the end of T wave in ECG measurement, which is the end of ventricular systole. Based on the aforementioned analysis, the fine-grained movements of atria and ventricles captured by mmWave could roughly match the ECG measurement to exhibit the cardiac cycles. Therefore, it is feasible to leverage

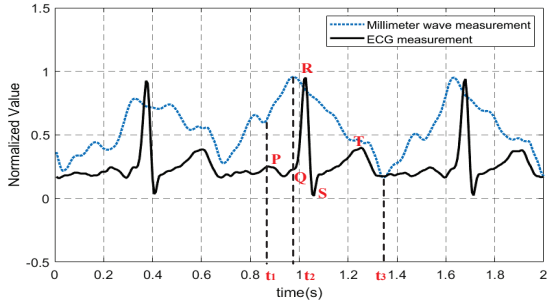

Fig. 3. Comparison of ECG measurement and mmWave measurement.

mmWave-based FMCW radar for capturing the fine-grained heart movements, and further determine the stages of atria and ventricles for the diagnosis.

According to the study above, the fine-grained movements of atria and ventricles could be captured by mmWave signals in a static environment without the existence of other body movements. However, in driving environments, there are various movements such as driving operations, breathing and heartbeat of drivers, dynamics of vehicles, etc., and all the movements cause phase changes in mmWave signals. Therefore, our goal is to eliminate interferences from other movements in dynamic driving environments and extract fine-grained heart movements of drivers.

III. System Design

A. System Overview

We devise a fine-grained cardiac cycle monitoring system, mmECG, which estimates minute heart movements of drivers in driving environments leveraging mmWave signals. Figure 4 shows the system architecture of mmECG. The whole system consists of three steps: *mmWave Signal Pre-processing*, *Basic Heart Movements Estimation* and *Cardiac Cycle Reconstruction*. In *mmWave Signal Pre-processing*, we design the chirp mmWave signal to achieve satisfactory distance and time resolutions for cardiac cycle monitoring. The designed mmWave signal is transmitted to drivers and reflected signals are captured by the same radar. Then, the phase changes in mmWave signals caused by all the movements in driving environments are calculated from the received signal. Afterwards, in *Basic Heart Movements Estimation*, a movement mixture model is constructed to represent the phase changes of mmWave signals caused by all the movements in driving environments. Based on the model, a hierarchical Variational Mode Decomposition (VMD) approach is designed to separate the interferences from the phase changes induced by heart movements based on their unique frequency characteristics. Finally, in *Cardiac Cycle Reconstruction*, mmECG segments the extracted phase changes into cardiac cycles utilizing shape similarity of heartbeats in mmWave signals, and further leverages a template-based optimization approach to reconstruct the atrial and ventricular stages in each cardiac cycle.

B. mmWave Signal Pre-processing

mmECG first pre-processes mmWave signals to detect subtle movements of objects.

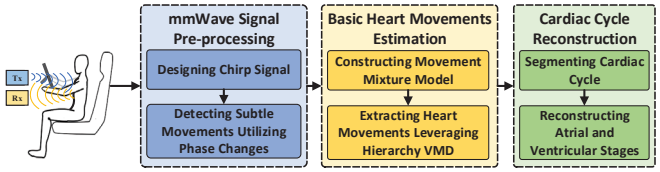

Fig. 4. System architecture of mmECG.

Designing Sensing Signal. mmECG employs the mmWave-based radar to detect the skin vibrations of human chest induced by heartbeats for cardiac cycle monitoring. Specifically, the radar leverages FMCW technique to transmit chirps with linearly increased frequency from the transmitting antennas, and then utilizes the receiving antennas to collect the reflected signals. After that, the radar would mix the transmitted and received FMCW signals to generate the Intermediate Frequency (IF) signal, which embeds all the information sensed by the radar, including the cardiac cycles.

Subtle Movements Detection. To capture the subtle movements of cardiac cycles, mmECG derives phase changes of mmWave signals from the IF signal. Specifically, mmECG performs FFT operation (Range-FFT) on the IF signal to obtain a *Range-Profile* for the target.

Based on the range profile, the phase changes of successive chirps in FMCW signals are calculated to detect the subtle heart movements. Theoretically, the sampled mmWave signal $s(d,k)$ after the FFT operation is $S(d,k) = r(d,k) + i(d,k) \cdot j$, where $r(d,k)$ and $i(d,k)$ are the real and imaginary parts of the mmWave signal respectively, d and k are the distance bin and label of chirps of the signal respectively, j is the imaginary unit. Hence, the phase change $\Delta\phi(d,k)$ is derived as

$$\Delta\phi(d,k) = \arctan \frac{i(d,k)}{r(d,k)}. \tag{1}$$

Hence, with the phase change, mmECG could achieve the sub-millimeter level movement detection in each distance bin.

C. Basic Heart Movements Estimation

Since mmECG achieves sub-millimeter level movements detection after signal preprocessing, all movements of a driver in driving environments, including driving operations (e.g., steering and braking), subtle body movements (e.g., breathing and heartbeat) and vibrations brought by driving, could be captured by the phase changes of mmWave signal. However, the phase changes caused by a movement located in a certain distance bin could influence several adjacent distance bins. In other words, when there are multiple movements at the same time, each distance bin contains the phase changes caused by a mixture of movements. Thus, even different movements happen in different distance bins with respect to the mmWave sensor, we can not directly distinguish each movement according to distance.

To extract heart movements from phase changes of mmWave signal, we first construct a movement mixture model to represent the transitivity of phase changes brought by all the movements. Then, based on the constructed model, we design a hierarchy VMD approach to separate different movements from the phase changes in mmWave signals and further estimate basic heart movements.

1) Constructing Movement Mixture Model: We first exploit the transitivity of phase changes in mmWave signal. As an electromagnetic wave, after been transmitted by the mmWave sensor, mmWave signal in the space within the sensing range forms a mmWave field, which is a physical field of mmWave energy. When there is a movement in the space, it stirs the mmWave field and cause the spread of the mmWave signal, just like the spread of ripple.

Thus, the phase changes of mmWave signals caused by movements can be transitive among different range bins. Based on the transitivity of phase changes, we further model the phase changes in each distance bin as a linear mixture of different movements. Specifically, for a time unit and N distance bins, given K movements $M_1, M_2, \ldots, M_K$ and the phase changes of each movement in the corresponding movement bin $C_1, C_2, \ldots, C_K$, the phase changes in a distance bin $B_n, n \in 1, 2, \ldots, N$, are denoted as:

$$P_{B_n} = \sum_{i=1}^{K} \alpha_{in} C_i, \tag{2}$$

where α_{in} is the attenuation coefficient of the phase changes caused by the movement M_i in distance bin B_n, which satisfies $\alpha_{in} \in [0,1]$. Therefore, the phase changes extracted from mmWave signals can be modeled as a mixture of the phase changes induced by different movements, which can be represented by:

$$P_{B(N\times 1)} = \alpha_{(N\times K)} \times C_{(K\times 1)}, \tag{3}$$

modulated by the attenuation coefficient matrix α.

2) Separating Movements Leveraging Hierarchy VMD: According to the constructed movement mixture model, estimating the heart movement of a driver from the mmWave signal is to find out the phase changes caused by the heart movement in the distance bin related to the chest of the driver. Although we could obtain the overall phase changes of all movements in each distance bin, i.e., P_B, from mmWave signal based on the movement mixture model, the phase changes C can not be calculated from Eq.3 because the attenuation matrix α is unknown.

To obtain the phase changes caused by the heart movement of drivers, we need to separate all the movements in the sensing range of mmWave sensor in driving environments. Typically, there are four main categories of independent movements in driving environments: 1) Operations of drivers, which refer to movements of driving operations (such as steering and braking), with large moving range (sub-meter-level) and relatively low frequency (0.1-2Hz). 2) Breathing of drivers, with medium moving ranges (centimeter-level) and medium frequency (0.16-0.6Hz) [14]. 3) Heartbeat of drivers, with small moving ranges (millimeter and sub-millimeter-level) and relatively high frequency (0.7-3.5Hz) [15]. 4) Vibrations in the driving environments, with different range and frequencies according to the level of vibrations. Since four categories of

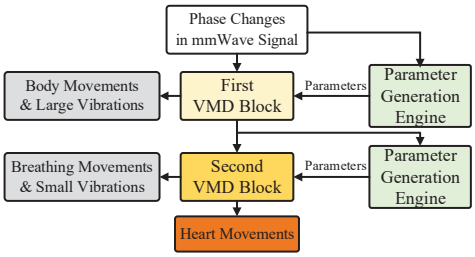

(a) Hierarchy VMD Architecture.

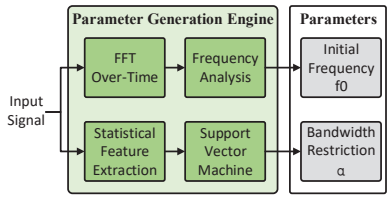

(b) Parameter Generation Engine Architecture.

Fig. 5. Illustration of hierarchy VMD approach.

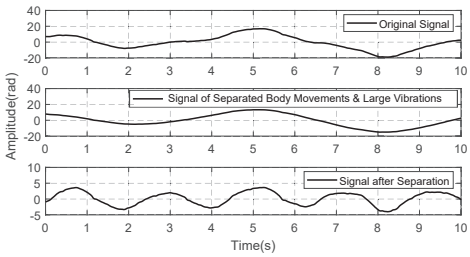

(a) Illustration of first VMD result.

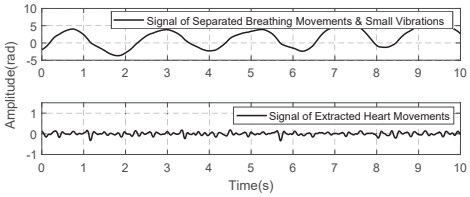

(b) Illustration of second VMD result.

Fig. 6. Illustration of hierarchy VMD result on a 10s mmWave signal.

movements have different but overlapped frequency ranges, simply applying band-pass filter may not works to separate different movements. Thus, we consider applying Variational Mode Decomposition (VMD) approach [16], which works as a self-adaptive filter to decompose a mixed signal into different modes, to fit the requirements of movements separation in mmWave signal.

When applying VMD method, there are key parameters to be determined ahead to ensure the performance of decomposition, including the number of components k, the bandwidth restriction of components α and the initial frequency of each components f_0. Moreover, since the four categories of movements have very different ranges both in amplitude and frequency, there can hardly be a combination of the parameters that could separate all four movements well at once. In order to deal with the issue and extract the phase changes related to the heart movements, we design a hierarchy VMD approach, to separate the movements step by step, as shown in figure 5. There are two VMD blocks in the hierarchy VMD approach, the first block is to separate the movements causing large amplitude changes of phase in mmWave signals, including behaviors of drivers and large vibrations of vehicles. And the second block is to separate movements bringing small amplitude of phase changes, such as breathing and small vehicle vibrations, leaving the phase changes of heart movements. For both blocks, the number of components k is set as 2 to separate one components from the mmWave signal. And the bandwidth restriction of components α and the initial frequency of the target component f_0 are determined automatically by the parameter generation engine, which takes the phase changes of mmWave signal as input, and outputs the parameters α and f_0 for the corresponding VMD block.

Figure 5(b) shows the detailed architecture of the parameter generation engine. The engine has two pipelines to generate the initial frequency f_0 and the bandwidth restriction of components α, respectively. For the initial frequency f_0, after receiving the phase changes in mmWave signal as input, the engine performs FFT to the phase changes over time to turn the phase changes into frequency domain. Then, the engine analyzes the frequency components and chooses the component with largest value in frequency domain as the initial frequency f_0 of the VMD block. The intuition is that the VMD block always separate the component with the largest phase change amplitude in mmWave signals, and the initial frequency should be set close to the component in order to guarantee the separation performance.

As for the bandwidth restriction parameter α, the parameter describes the bandwidth restriction for the separated component. If α is too small, then the signal would be over-separated, and if α is too large, the signal would be under-separated. However, it is hard to determine whether the signal is over-separated or under-separated before the separation. So to determine the parameter α, we extract the statistic features, including the amplitude, variance, etc., from the input signal to train a SVM regressor for determining α. The SVM regressor is trained with 10 hour mmWave data and corresponding breathing and heartbeat ground-truth data collected from 5 participants in real driving environments. Then, both the parameter f_0 and α can be generated automatically by the parameter generation engine given the input signal.

Based on the generated parameters, the hierarchy VMD approach can separate the behaviors and breathing of the driver, as well as vehicle vibrations from the phase changes of mmWave signal and extract the heart movements. Figure 6 illustrates the result of hierarchy VMD on a 10s mmWave signal, which is collected in real driving environments. The signal of body movements is separated by the first VMD block from the original signal, as shown in figure 6(a). It can be seen that the signal after separation is clearly periodic, since it contains mainly the signal of breathing movements and heart movements. Using the signal after separation as the input of the second VMD block, the breathing movements is separated and the signal of heart movements is estimated, as shown in figure 6(b).

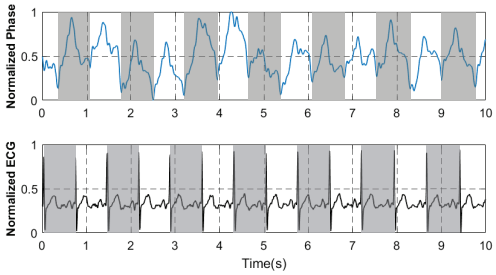

Fig. 7. Illustration of cardiac cycle segmentation.

D. Cardiac Cycle Reconstruction

After the basic heart movement is extracted from the phase changes of mmWave signals, mmECG reconstructs the implicit cardiac cycle behind the heart movements to estimate fine-grained movements of atria and ventricles.

1) Segmenting Cardiac Cycle: To reconstruct the cardiac cycle, mmECG first estimates the length of each cardiac cycle by segmenting the extracted phase changes of mmWave signals into pieces. Each segment relates to a cardiac cycle. The key insight is that, in spite of the subtle diversities of amplitude, frequency, etc., in each heartbeats of a driver, the general shape of successive human heartbeats are similar in the phase changes of mmWave signal. So the problem of cardiac cycle segmentation can be constructed as an optimization problem [4]. Specifically, mmECG aims to find a segmentation $S = \{s_1, s_2, \ldots, s_n, \ldots\}$ with the length of each segments $\{|s_1|, |s_2|, \ldots, |s_n|, \ldots\}$ that maximizes the similarity of each segments, which can be denoted as:

$$\arg\max_{S} \sum_{s_i, s_j \in S} cor(s_i, \omega(\mu, |s_i|)), \tag{4}$$

where μ is a template for the shape of an cardiac cycle in phase changes of mmWave signal. $\omega(\mu, |s_i|)$ re-samples template μ to the length of segment s_i, and $cor()$ is the correlation coefficient between template μ and segment s_i. Similar to [4], we leverage dynamic programming to solve the optimization problem, and get an segmentation of cardiac cycles as shown in figure 7. It can be seen that the length of the segments are very close to the ground truth of corresponding ECG measurements, except the time shift caused by the lack of calibration for cardiac cycles in Eq.4.

2) Reconstructing Atria and Ventricles Stages: Based on the segmentation of cardiac cycles, mmECG further reconstructs atrial and ventricular stages by determining the key time points in each cardiac cycle, which are the beginning time of atrial systole t_1, the end time of atrial systole and the beginning time of ventricular systole t_2, and the end time of ventricular systole t_3, as described in Section 2.3.

In order to realize the determination, we first design a template of atria and ventricles movements in the phase change of mmWave signal, and then apply an optimization method on the template to find the key time points t_1, t_2 and t_3 for each cardiac cycle in mmWave signals. To design the template, mmECG segments the phase changes in mmWave signals with purely heart movements based on peak detection method and

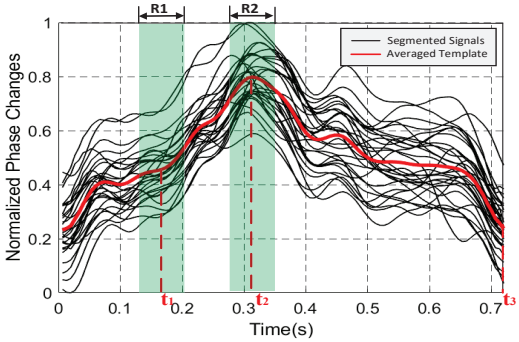

Fig. 8. Illustration of the template of cardiac cycle.

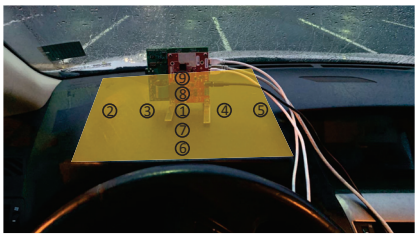

Fig. 9. Illustration of radar placements in driving environments.

re-samples each segment to the average length. After that, the segments are averaged to a template that represents a typical cardiac cycle, as shown in figure 8. It can be seen that t_3 is determined as the end time of a cardiac cycle, while t_1 and t_2 are the intermediate time points within the cardiac cycle. Since the relative time of t_1 and t_2 can be different in each cardiac cycle, we assume that t_1 and t_2 can move within the range R_1 and R_2, respectively. During the movements of t_1 and t_2, the overall length of template remains fixed, and the parts beside t_1 and t_2 scales accordingly.

Based on the template, we set the length of the template for the ith cardiac cycle L_{c_i} to be the same as the length of ith segmented cardiac cycles in figure 7, and then we slide the template $temp_i$ to calibration t_3 to the ith cardiac cycle c_i in figure 7. Within the template $temp_i$, mmECG further searches for the best position of t_1 and t_2 that maximizes the similarity between the cardiac cycle and the template,

$$\arg\max_{t_1, t_2, t_1 \in R1, t_2 \in R2} cor(c_i, temp_i), \tag{5}$$

where $cor(c_i, temp_i)$ represents the correlation coefficent between cardiac cycle c_i and dynamic template $temp_i$. By searching the range of R_1 and R_2 for t_1 and t_2, respectively, mmECG obtains the optimal solution for t_1 and t_2. Together with t_3, these three key time points of atrial and ventricular stages are determined by mmECG.

By reconstructing atrial and ventricular stages, mmECG could get medical-level heartbeat information of drivers, which could be helpful for the healthcare of drivers on roads.

IV. Evaluation

In this section, we evaluate the performance of *mmECG* under the collected data from 25 different volunteers in real driving environments.

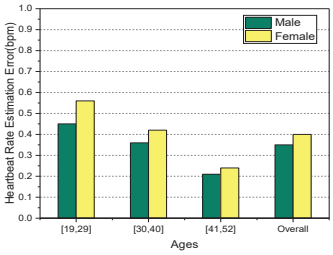

Fig. 10. Overall HR estimation.

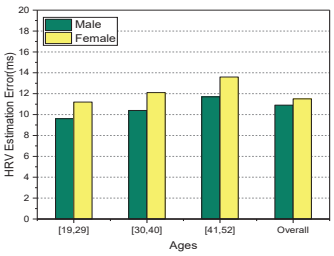

Fig. 11. Overall HRV estimation.

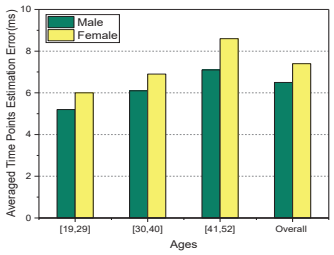

Fig. 12. Overall CC estimation.

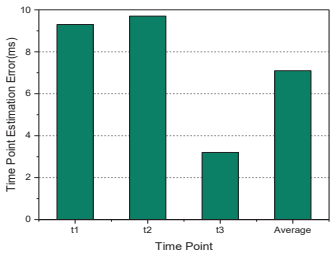

Fig. 13. Key points estimation error.

A. Experimental Setup and Methodologies

We implement mmECG with a commercial TI AWR1642 mmWave radar [17] as the sensing front end and a Dell XPS 13 laptop as the data processing back end. The mmWave radar is equipped with two on-board transmitter antennas and four receiver antennas, and is connected with a TI DCA1000EVM data capture card [18] to achieve the high-speed data transmission between the mmWave radar and laptop. On the other hand, we utilize a Heal Force PC-80B ECG monitor [19] to capture the ground truth of ECG measurement. The collected data and ground truth data are paired and separated into 30s-samples for further processing and evaluation.

In the experiments, the mmWave radar is placed in front of the volunteer driver on the dashboard of a car. Specifically, there are 9 different positions for sensor placement as illustrated in Figure.9. Within the 9 positions. The distance between mmWave radar and volunteer's chest is between $40cm$ and $80cm$. And the corresponding angle is in the range of $[-20°, 20°]$. During the experiments, we recruit 25 volunteers (14 males, 11 females, ages$[19, 52]$), and 3 different cars (Lexus RX350, BMW X3, Honda Accord). During experiment, each volunteer randomly drives a car in different road conditions including plain road, cobblestone street, and bumped road, which generate different kinds of dynamics. And we collect the measurements with mmECG under the aforementioned setups. In total, we collect about 200 hours data, which corresponds to 24000 samples.

We define several metrics for the evaluations.

• **Heart Rate(HR) Estimation Error**: The error of the estimated heart rate R_E from ground truth heart rate R_G measured by ECG devices, which is defined as the absolute difference between R_E and R_G, i.e., $\Delta_{HR} = |R_E - R_G|$.

• **Heart Rate Variation(HRV) Estimation Error**: The error of the RMSSD [20] of estimated heart movements $RMSSD_E$ from the RMSSD of ground truth measured by ECG devices $RMSSD_G$, i.e., $\Delta_{HRV} = |RMSSD_E - RMSSD_G|$, where $RMSSD = \sqrt{\frac{1}{N}\sum_{i=2}^{N}(IBI_i - IBI_{i-1})^2}$, in which IBI_i is the duration of the ith cardiac cycle.

• **Cardiac Cycle(CC) Estimation Error**: The error of the RMSSD of estimated key time points(i.e., t_1, t_2 and t_3) of each cardiac cycle from the RMSSD of ground truth measured by ECG devices. For instance, for time point t_1, the error is $\Delta_{t_1} = |RMSSD_E^{t_1} - RMSSD_G^{t_1}|$. For all three time points, the overall cardiac cycle estimation error is the average of the sum of three individual time points estimation error.

B. Overall Performance

We evaluate the overall performance of mmECG for different groups of volunteers. Since HR directly exhibits a coarse-grained result of heart movement estimation, we first estimate the HR based on the segmented cardiac cycles in mmECG. Figure 10 shows the heart rate(HR) estimation error of mmECG under different genders and age groups. It can be seen that HR estimation errors of all genders and age groups are lower than $0.6bpm$, showing that mmECG can achieve accurate HR estimation in driving environments. Figure 11 shows the heart rate variation(HRV) estimation error of mmECG. It can be seen that the HRV estimation errors for all genders and age groups are lower than $14ms$, indicating that mmECG can accurately estimate the HRV of drivers in driving environments. Figure 12 finally shows the cardiac cycle(CC) estimation error of mmECG. We can observe that the CC estimation errors for all genders and age groups are lower than $9ms$. Further, for each of the three key time points t_1, t_2 and t_3 in cardiac cycles, the estimation results are shown in figure 13. It can be observed that the estimation error for all the three key time points are lower than $10ms$, which is accurate enough to provide fine-grained heart movements information of drivers as a health indicator. It also can be seen from figure 13 that the estimation error of t_3 is lower than t_1 and t_2, which is because that t_3 has more robust shape characteristic as the ending time point of each cardiac cycle in mmWave signals.

Moreover, for females, their estimation errors of HR, HRV and CC are slightly higher than that of males as shown in figure 10, 11 and 12, because the average heartbeat rates of woman is higher than that of man [21]. Meanwhile, the estimation errors of younger volunteers for HR estimation (as shown in figure 10) are slightly higher than that of older volunteers, but are slightly lower than that of older volunteers in HRV estimation (as shown in figure 11) and CC estimation (as shown in figure 12). The reason is that HR of younger people are usually higher than older people [9], which brings more variations on HR estimation. For HRV and cardiac cycles, the higher heart rate brings short time for each cardiac cycle, resulting in lower estimation errors. Overall, mmECG could achieve accurate estimation for all of the three kinds of measurements, i.e., HR, HRV and CC estimation. Since CC estimation exhibits finer-grained cardiac cycle results compared with HR and HRV, the following evaluations focus on showing the CC estimation error for evaluating the performance of mmECG.

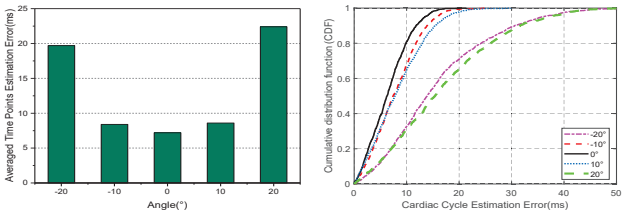

(a) Average CC estimation error. (b) CDF of CC estimation error.

Fig. 14. Performance under different angles.

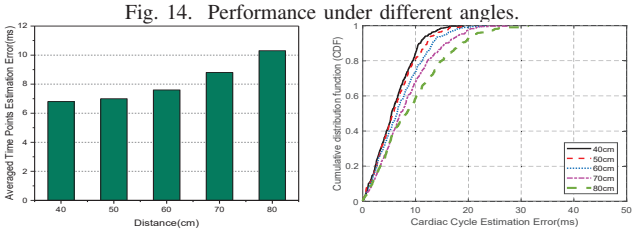

(a) Average CC estimation error. (b) CDF of CC estimation error.

Fig. 15. Performance under different distances.

C. Impact of mmWave Radar Placements

Figure 14(a) shows the average CC estimation error under different angles of the mmWave radar with respect to drivers. It can be seen that the lowest estimation error is achieved at the angle of $0°$. When the angle goes far from $0°$, the error increases, specially after the angle being $\pm 20°$. This is because the small wavelength of mmWave induces the narrow main beam, indicating a highly-directional field-of-view of the mmWave radar (i.e., within the angle range $[-15°, 15°]$ [17]). When the driver's body gets close to the boundary of the field-of-view, the sideband of the mmWave signal has much less power, leading to dramatical performance degradation. Figure 14(b) further shows the CDF of CC estimation error under different angles. It can be seen that when the angle is within the range of $[-15°, 15°]$, more than 80% errors are lower than 14ms. Considering the width that the mmWave radar can cover is $46cm$ (i.e., with the angle of $[-15°, 15°]$ and distance of $40cm$), which is much wider than the width of a human body indicating that mmECG could accurately monitor a driver's cardiac cycle with a reasonable setup.

We also evaluate the impact of distance between mmWave radar and human chest on mmECG. Figure 15(a) shows the average CC estimation error under different distance of the mmWave radar with respect to drivers, and the corresponding CDF of CC estimation errors are plotted in figure 15(b). It can be observed that when the distance is within $80cm$, which is natural in driving environments, the averaged CC estimation error is no more than $12ms$, and the CC estimation error is lower than $20ms$ for more than 90% cases. The result shows that mmECG could accurately monitor the cardiac cycle with under available distances in driving environments.

D. Impact of Heart Rates

Since heart rate could influence the duration of each cardiac cycle directly, we thus evaluate the impact of heart rates of drivers on the performance of mmECG. Figure 16(a) shows the averaged CC estimation error under different heartbeats of drivers, and figure 16(b) plots the corresponding CDF

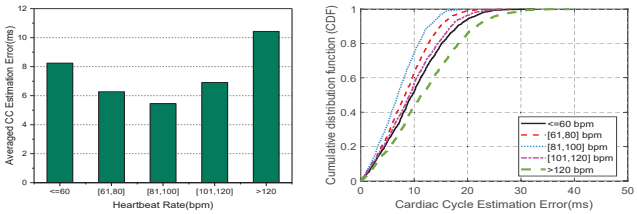

(a) Average CC estimation error. (b) CDF of CC estimation error.

Fig. 16. Performance of mmECG under different heart rates of drivers.

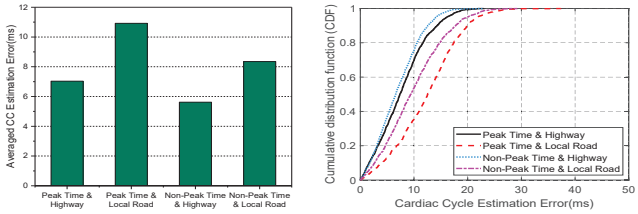

(a) Average CC estimation error. (b) CDF of CC estimation error.

Fig. 17. Performance of mmECG under different road types and traffic conditions.

of CC estimation error. It can be seen that mmECG could achieve averaged CC estimation error lower than $11ms$ under all heart rates of drivers, with CC estimation error less than $20ms$ for more than 80% samples, showing that mmECG could accurately estimate the cardiac cycles of drivers under different heart rates. Moreover, when the heart rate of drivers increases from slow(i.e., $<= 60bpm$) to fast(i.e., $> 120bpm$), the averaged CC estimation error first decreases and then increases. As we know the higher heart rate the higher heart rate brings shorter duration for each cardiac cycle, resulting to lower estimation error brought by variation. And the reason that the errors increase when drivers' heart rates are higher than $100bpm$ is because the breathing movements are normally become heavy when the heart rates are very high, which decrease the SNR of heart movements in mmWave signals, and further increase the estimation error of mmECG.

E. Impact of Traffic Conditions

Traffic conditions may influent drivers' driving behaviors and vehicle conditions, thus could impact the performance of mmECG. We analyze the collected traces of different traffic conditions (during peak time and off-peak time) and different road types (on local road and highway), respectively. Figure 17(a) and 17(b) show the averaged CC estimation error and CDF of CC estimation error under all four combinations of road types and traffic conditions, respectively. It can be seen that the averaged CC estimation error is lower than $11ms$ and the CC estimation error is lower than $18ms$ for more than 80% samples under any combination of road types and traffic conditions. Moreover, during peak time, the estimation error is slightly larger because drivers may perform more driving operations during heavy traffic, which brings interferences to mmECG. For different road types, the estimation error on local roads is slightly larger because on local roads, vehicles may suffer from poor road conditions, such as bumpy roads, which brings extra interferences.

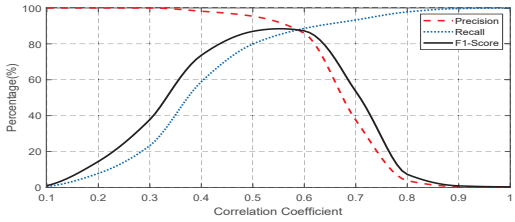

Fig. 18. Performance of mmECG on abnormal heartbeat detection.

F. Abnormality Detection Performance

We also evaluate the performance of mmECG on abnormal heartbeat detection, such as atrial fibrillation. For this experiment, we develop an additional function to detect the abnormal heartbeats. As mentioned in Section III-D, mmECG employs a template built by pre-collected normal heartbeats for cardiac cycles reconstruction. Based on the template indicating normal heartbeats, mmECG could detect the abnormal heartbeats by calculating the correlation between the detected cardiac cycle and the template. If this correlation is less than a threshold δ, the detected cardiac cycle would be considered as abnormal. Also, to collect the ground truth, we invite professional physicians to diagnose the collected ECG samples for figuring out the abnormal heartbeats. Among the $240,00$ collected samples, 381 of them are considered abnormal.

Figure 18 shows the performance of mmECG on abnormal heartbeat detection under different thresholds δ. It can be observed that as the δ increases from 0.1 to 1, the precision of abnormal heartbeat detection first keeps as 100% when δ is smaller than 0.32 and then decreases to 0, while the recall of abnormal heartbeat detection increases from 0 to 100%. And the F1-score, which combines precision and recall, first increases until $\delta = 0.55$ and then decreases. Therefore, mmECG sets $\delta = 0.55$ for the threshold selection, which corresponds to the 88.9% for the F1-score of abnormal heartbeat detection. The results show that mmECG can effectively monitor the health state of drivers.

V. Related Work

In this section, we review the key researches about mmWave sensing and vital sign detection.

mmWave Sensing Background. The mmWave techniques have been employed for sensing human gestures [22], [23], indoor localization and floor map constructions [24]–[27], enabling precise navigation functions for indoor environments. Further researches also investigate the feasibility of using mmWave in authenticating user identity [28] or lip reading [29]. All of these studies demonstrate the feasibility of extending mmWave to sensing areas. Along this direction, we are motivated to realizing the fine-grained heartbeat monitoring leveraging mmWave techniques.

Vital Sign Detection. Some researches monitor the coarse-grained breathing for health monitoring, such as breathing rate and events for daily and sleep monitoring respectively. For example, some work [30], [31] employ smartwatches to track one's breathing for health monitoring. However, such a monitoring manner introduces intrusive experience. To improve the user experience, other researches realize the breathing monitoring systems using wireless signals, such as commercial WiFi [32], low-cost RFID [33], [34], and audio devices [35]–[37].

Some other researches focus on detecting heartbeats for health monitoring. Early work [38] develops dedicated infrastructures to achieve the heartbeats monitoring. To reduce the cost for widely deployments, some other studies integrate advanced signal processing techniques into COTS devices to provide the capability of heartbeats monitoring. For example, some researches realize the heartbeats monitoring systems using commercial WiFi [6], low-cost RFID [7], audio devices [8], and even mmWave [39]. Another work [4] even realizes the emotion recognition system by monitoring one's heartbeats through RFID signals. However, due to the limited resolution of COTS devices, the heartbeats monitoring can only realize the heart rate measurements, which is far from the professional diagnosis under specialized infrastructures. Furthermore, all the aforementioned researches require the users to maintain a static posture, which hardly supports various conditions, especially the driving environments with consistent vibrations. Most recently, a few researches start to focus on heartbeats monitoring under dynamic environments [40] [41], but they still can not reach information finer than heart rates or HRV measurements.

Different from aforementioned researches, our work aims to monitor the cardiac cycles represented as the systole and diastole movements of atrial and ventricular under dynamic environments, instead of the brief heart rates or HRV measurements, to support the health monitoring. The most related works are seismocardiography monitoring using RF signals [42] [43] [44], these works focus on the seismocardiography reconstruction, which is parallel to our work.

VI. Conclusion

In this paper, we propose a cardiac cycle monitoring system, mmECG, which leverages the COTS mmWave radar to monitor the cardiac cycle of drivers for potential healthcare services in driving environments. mmECG first designs FMCW-based mmWave signals to detect the heart movements of drivers as phases changes in mmWave signals. Based on the detected phase changes, a movement mixture model is constructed and the phase changes caused by heart movements are extracted with a hierarchy variational mode decomposition(VMD) approach. Finally, mmECG applies a template-based optimization estimating fine-grained movements of atria and ventricles based on the extracted phase changes. The experiments under real driving environments validate the performance of mmECG on cardiac cycle monitoring.

Acknowledgment

This research was sponsored by NSFC (No.62172277), CCF-AFSGRF20200013, and STCSM (Science and Technology Commission of Shanghai Municipality) AI project (No. 19511120300).

REFERENCES

[1] W. Kim, V. Anorve, and B. Tefft, "American driving survey, 2014–2017," 2019.

[2] B. Roman, S. Pavel, P. Miroslav, V. Petr, and P. Lubomír, "Fatigue indicators of drowsy drivers based on analysis of physiological signals," in *International Symposium on Medical Data Analysis*. Springer, 2001, pp. 62–68.

[3] N. Egelund, "Spectral analysis of heart rate variability as an indicator of driver fatigue," *Ergonomics*, vol. 25, no. 7, pp. 663–672, 1982.

[4] M. Zhao, F. Adib, and D. Katabi, "Emotion recognition using wireless signals," in *Proceedings of ACM MobiCom*, New York City, NY, USA, 10 2016, pp. 95–108.

[5] X. Zhang, W. Li, X. Chen, and S. Lu, "Moodexplorer: Towards compound emotion detection via smartphone sensing," *Proceedings of the ACM on Interactive, Mobile, Wearable and Ubiquitous Technologies*, vol. 1, no. 4, pp. 1–30, 2018.

[6] J. Liu, Y. Wang, Y. Chen, J. Yang, X. Chen, and J. Cheng, "Tracking vital signs during sleep leveraging off-the-shelf wifi," in *Proceedings of ACM MobiHoc*, Hangzhou, China, 6 2015, pp. 267–276.

[7] F. Adib, H. Mao, Z. Kabelac, D. Katabi, and R. C. Miller, "Smart homes that monitor breathing and heart rate," in *Proceedings of ACM CHI*, Seoul, Republic of Korea, 4 2015, pp. 837–846.

[8] K. Qian, C. Wu, F. Xiao, Y. Zheng, Y. Zhang, Z. Yang, and Y. Liu, "Acousticcardiogram: Monitoring heartbeats using acoustic signals on smart devices," in *Proceedings of IEEE INFOCOM*, Honolulu, HI, USA, 4 2018, pp. 1574–1582.

[9] K. E. Barrett, *Ganong's review of medical physiology*. McGraw Hill Education, 2019, no. 1.

[10] L. S. Lilly, *Pathophysiology of heart disease: a collaborative project of medical students and faculty*. Lippincott Williams & Wilkins, 2012.

[11] G. J. Tortora and B. H. Derrickson, *Principles of anatomy and physiology*. John Wiley & Sons, 2018.

[12] T. Wu, T. S. Rappaport, and C. M. Collins, "The human body and millimeter-wave wireless communication systems: Interactions and implications," in *2015 IEEE International Conference on Communications (ICC)*. IEEE, 2015, pp. 2423–2429.

[13] F. G. Yanowitz, "Introduction to ecg interpretation," in *LDS Hospital & Intermountain Medical Center, Salt Lake City*, 2012.

[14] J. P. Mortola, "Breathing around the clock: an overview of the circadian pattern of respiration," *European journal of applied physiology*, vol. 91, no. 2-3, pp. 119–129, 2004.

[15] B. Nes, I. Janszky, U. Wisløff, A. Støylen, and T. Karlsen, "Age-predicted maximal heart rate in healthy subjects: The hunt f itness s tudy," *Scandinavian journal of medicine & science in sports*, vol. 23, no. 6, pp. 697–704, 2013.

[16] K. Dragomiretskiy and D. Zosso, "Variational mode decomposition," *IEEE transactions on signal processing*, vol. 62, no. 3, pp. 531–544, 2013.

[17] TI, "Awr1642 single-chip 77- and 79-ghz fmcw radar sensor," [Online]. Available: https://www.ti.com/lit/ds/symlink/awr1642.pdf, 2019.

[18] TI, "Real-time data-capture adapter for radar sensing evaluation module," [Online]. Available: https://www.ti.com/tool/DCA1000EVM?HQS=TI-null-null-digikeymode-df-pf-null-wwe, 2019.

[19] H. Force, "Pc-80b," [Online]. Available: http://www.healforce.com/cn/index.php?ac=article, 2020.

[20] F. Shaffer and J. Ginsberg, "An overview of heart rate variability metrics and norms," *Frontiers in public health*, vol. 5, p. 258, 2017.

[21] K. Prabhavathi, K. T. Selvi, K. Poornima, and A. Sarvanan, "Role of biological sex in normal cardiac function and in its disease outcome–a review," *Journal of clinical and diagnostic research: JCDR*, vol. 8, no. 8, p. BE01, 2014.

[22] J. Lien, N. Gillian, M. E. Karagozler, P. Amihood, C. Schwesig, E. Olson, H. Raja, and I. Poupyrev, "Soli: ubiquitous gesture sensing with millimeter wave radar," *ACM Transactions on Graphs*, vol. 35, no. 4, pp. 142:1–142:19, 7 2016.

[23] T. Wei and X. Zhang, "mtrack: High-precision passive tracking using millimeter wave radios," in *Proceedings of ACM MobiCom*, Paris, France, 9 2015, pp. 117–129.

[24] J. Palacios, G. Bielsa, P. Casari, and J. Widmer, "Communication-driven localization and mapping for millimeter wave networks," in *Proceedings of IEEE INFOCOM*, Honolulu, HI, USA, 4 2018, pp. 2402–2410.

[25] J. Palacios, P. Casari, H. Assasa, and J. Widmer, "LEAP: location estimation and predictive handover with consumer-grade mmwave devices," in *Proceedings of IEEE INFOCOM*, Paris, France, 4 2019, pp. 2377–2385.

[26] J. Palacios, P. Casari, and J. Widmer, "JADE: zero-knowledge device localization and environment mapping for millimeter wave systems," in *Proceedings of IEEE INFOCOM*, Atlanta, GA, USA, 5 2017, pp. 1–9.

[27] A. Zhou, S. Yang, Y. Yang, Y. Fan, and H. Ma, "Autonomous environment mapping using commodity millimeter-wave network device," in *Proceedings of IEEE INFOCOM*, Paris, France, 4 2019, pp. 1126–1134.

[28] P. Zhao, C. X. Lu, J. Wang, C. Chen, W. Wang, N. Trigoni, and A. Markham, "mid: Tracking and identifying people with millimeter wave radar," in *Proceedings of DCOSS*, Santorini, Greece, 5 2019, pp. 33–40.

[29] C. Xu, Z. Li, H. Zhang, A. S. Rathore, H. Li, C. Song, K. Wang, and W. Xu, "Waveear: Exploring a mmwave-based noise-resistant speech sensing for voice-user interface," in *Proceedings of ACM MobiSys*, Seoul, Republic of Korea, 6 2019, pp. 14–26.

[30] X. Sun, L. Qiu, Y. Wu, Y. Tang, and G. Cao, "Sleepmonitor: Monitoring respiratory rate and body position during sleep using smartwatch," *Proceedings of the ACM on Interactive, Mobile, Wearable and Ubiquitous Technologies*, vol. 1, no. 3, pp. 104:1–104:22, 9 2017.

[31] Y. Zhang, Z. Yang, Z. Zhang, P. Li, D. Cao, X. Liu, J. Zheng, Q. Yuan, and J. Pan, "Breathing disorder detection using wearable electrocardiogram and oxygen saturation," in *Proceedings of ACM SenSys*, Shenzhen, China, 11 2018, pp. 313–314.

[32] P. Nguyen, X. Zhang, A. C. Halbower, and T. Vu, "Continuous and fine-grained breathing volume monitoring from afar using wireless signals," in *Proceedings of IEEE INFOCOM*, San Francisco, CA, USA, 4 2016, pp. 1–9.

[33] Y. Hou, Y. Wang, and Y. Zheng, "Tagbreathe: Monitor breathing with commodity RFID systems," in *Proceedings of IEEE ICDCS*, Atlanta, GA, USA, 6 2017, pp. 404–413.

[34] R. Zhao, D. Wang, Q. Zhang, H. Chen, and A. Huang, "CRH: A contactless respiration and heartbeat monitoring system with COTS RFID tags," in *Proceedings of IEEE SECON*, Hong Kong, China, 6 2018, pp. 325–333.

[35] H. E. Romero, N. Ma, G. J. Brown, A. V. Beeston, and M. Hasan, "Deep learning features for robust detection of acoustic events in sleep-disordered breathing," in *Proceedings of IEEE ICASSP*, Brighton, United Kingdom, 5 2019, pp. 810–814.

[36] X. Xu, J. Yu, Y. Chen, Y. Zhu, L. Kong, and M. Li, "Breathlistener: Fine-grained breathing monitoring in driving environments utilizing acoustic signals," in *Proceedings of ACM MobiSys*, Seoul, Republic of Korea, 6 2019, pp. 54–66.

[37] Y. Ren, C. Wang, Y. Chen, J. Yang, and H. Li, "Noninvasive fine-grained sleep monitoring leveraging smartphones," *IEEE Internet of Things Journal*, vol. 6, no. 5, pp. 8248–8261, 6 2019.

[38] N. Jähne-Raden, M. Marschollek, U. Kulau, and L. C. Wolf, "Heartbeat the odds: A novel digital ballistocardiographic sensor system," in *Proceedings of ACM SenSys*, Delft, Netherlands, 11 2017, pp. 59:1–59:2.

[39] Z. Yang, P. H. Pathak, Y. Zeng, X. Liran, and P. Mohapatra, "Monitoring vital signs using millimeter wave," in *Proceedings of ACM MobiHoc*, Paderborn, Germany, 7 2016, pp. 211–220.

[40] Z. Chen, T. Zheng, C. Cai, and J. Luo, "MoVi-Fi: Motion-robust Vital Signs Waveform Recovery via Deep Interpreted RF Sensing," in *Proc. of the 27th ACM MobiCom*, 2021, pp. 392–405.

[41] T. Zheng, Z. Chen, C. Cai, J. Luo, and X. Zhang, "V2ifi: in-vehicle vital sign monitoring via compact rf sensing," in *Proc. of the 22nd ACM UbiComp*, 2020, pp. 70:1–27.

[42] Y. Li, Z. Xia, and Y. Zhang, "Standalone systolic profile detection of non-contact scg signal with lstm network," *IEEE Sensors Journal*, vol. 20, no. 6, pp. 3123–3131, 2019.

[43] C. Will, K. Shi, S. Schellenberger, T. Steigleder, F. Michler, J. Fuchs, R. Weigel, C. Ostgathe, and A. Koelpin, "Radar-based heart sound detection," *Scientific reports*, vol. 8, no. 1, pp. 1–14, 2018.

[44] U. Ha, S. Assana, and F. Adib, "Contactless seismocardiography via deep learning radars," in *Proceedings of the 26th Annual International Conference on Mobile Computing and Networking*, 2020, pp. 1–14.